Volume 9
Number 1
January 2022
Pages 1–510

Materials Horizons

rsc.li/materials-horizons

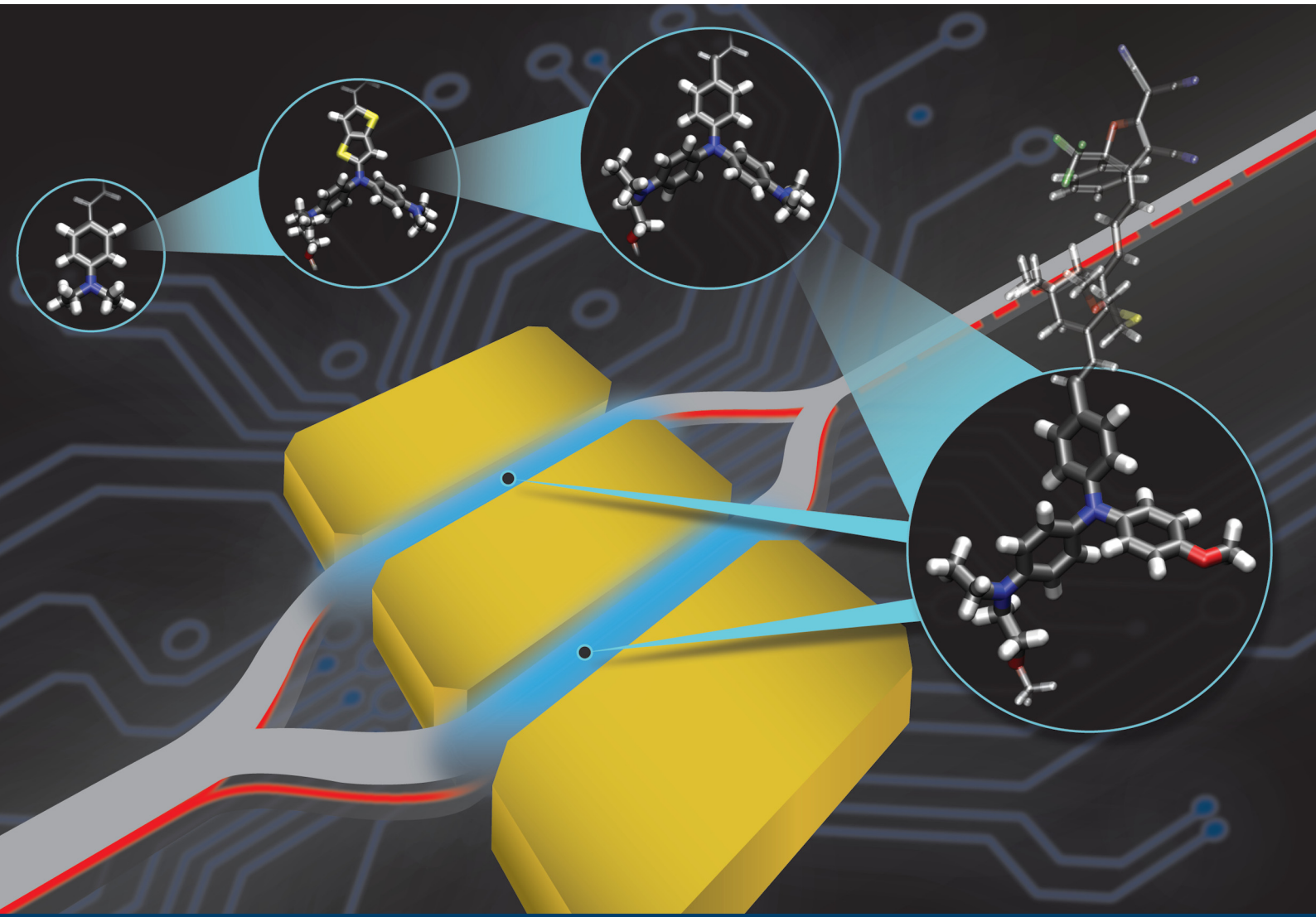

Special issue in honour of Seth Marder

ISSN 2051-6347

ROYAL SOCIETY OF CHEMISTRY

COMMUNICATION
Delwin L. Elder, Lewis E. Johnson *et al.*
Design and synthesis of chromophores with enhanced electro-optic activities in both bulk and plasmonic–organic hybrid devices

Materials Horizons

ROYAL SOCIETY OF CHEMISTRY

COMMUNICATION

View Article Online
View Journal | View Issue

Cite this: *Mater. Horiz.*, 2022, 9, 261

Received 30th July 2021,
Accepted 23rd September 2021

DOI: 10.1039/d1mh01206a

rsc.li/materials-horizons

Design and synthesis of chromophores with enhanced electro-optic activities in both bulk and plasmonic–organic hybrid devices†

Huajun Xu, [a] Delwin L. Elder, *[ab] Lewis E. Johnson, *[ab] Wolfgang Heni, [cd] Yovan de Coene, [e] Eva De Leo, [cd] Marcel Destraz, [cd] Norbert Meier, [c] Wouter Vander Ghinst, [e] Scott R. Hammond, [ab] Koen Clays, [e] Juerg Leuthold, [cd] Larry R. Dalton [a] and Bruce H. Robinson [a]

This study demonstrates enhancement of in-device electro-optic activity *via* a series of theory-inspired organic electro-optic (OEO) chromophores based on strong (diarylamino)phenyl electron donating moieties. These chromophores are tuned to minimize trade-offs between molecular hyperpolarizability and optical loss. Hyper-Rayleigh scattering (HRS) measurements demonstrate that these chromophores, herein described as BAH, show >2-fold improvement in β *versus* standard chromophores such as JRD1, and approach that of the recent BTP and BAY chromophore families. Electric field poled bulk devices of neat and binary BAH chromophores exhibited significantly enhanced EO coefficients (r_{33}) and poling efficiencies (r_{33}/E_p) compared with state-of-the-art chromophores such as JRD1. The neat BAH13 devices with charge blocking layers produced very large poling efficiencies of 11.6 ± 0.7 nm^2 V^{-2} and maximum r_{33} value of 1100 ± 100 pm V^{-1} at 1310 nm on hafnium dioxide (HfO_2). These results were comparable to that of our recently reported BAY1 but with much lower loss (extinction coefficient, k), and greatly exceeding that of other previously reported OEO compounds. 3 : 1 BAH-FD : BAH13 blends showed a poling efficiency of 6.7 ± 0.3 nm^2 V^{-2} and an even greater reduction in k. 1 : 1 BAH-BB : BAH13 showed a higher poling efficiency of 8.4 ± 0.3 nm^2 V^{-2}, which is approximately a 2.5-fold enhancement in poling efficiency *vs.* JRD1. Neat BAH13 was evaluated in plasmonic–organic hybrid (POH) Mach–Zehnder modulators with a phase shifter length of 10 μm and slot widths of 80 and 105 nm. In-device BAH13 achieved a maximum r_{33} of 208 pm V^{-1} at 1550 nm, which is ~1.7 times higher than JRD1 under equivalent conditions.

New concepts

Over the past decade, trade-offs among molecular hyperpolarizability (β), optical loss, number density (ρ_N), and electric field poling-induced acentric order ($\langle\cos^3\theta\rangle$) of organic electro-optic (OEO) chromophores have frequently stymied improvement of in-device EO activity. New chromophores that are designed for an improved molecular hyperpolarizabity would suffer unacceptable optical loss or severe adverse dipolar aggregations. Most of the previous work of organic EO chromophore design is mainly focused on improving ordering by means of side-chain engineering or chromophore blending, as well as increasing chromophore number density. Here we adopt a theory-guided design process including quantum mechanical and statistical mechanical techniques to design a new generation of organic EO materials relevant to silicon–organic hybrid (SOH) and plasmonic–organic hybrid (POH) devices. Theory-guided design allows for screening of many structures by evaluating their calculated hyperpolarizabilities, band gaps, and dipole moments, and optimizing targets for multiple design criteria. As a result, the newly designed chromophores in this work present enhanced hyperpolarizabilities and EO activities in both bulk devices and POH modulators without unacceptable impacts on processibility or loss. These results demonstrate that the hyperpolarizability-loss-processibility trade-off is not insurmountable and can be effectively addressed by theory-guided design, which could lead to even higher performance OEO materials for applications in nanophotonic devices.

1. Introduction

High-performance electro-optic (EO) modulators are key components for pushing the boundaries of optical communication,

[a] *Department of Chemistry, University of Washington, Seattle, WA 98195, USA. E-mail: lewisj@uw.edu, elderdl@uw.edu*
[b] *Nonlinear Materials Corporation, Seattle, WA 98109, USA*
[c] *Polariton Technologies AG, 8803 Rüschlikon, Switzerland*
[d] *Institute of Electromagnetic Fields, ETH Zurich, Gloriastrasse 35, Zurich 8092, Switzerland*
[e] *Department of Chemistry, University of Leuven, Celestijnenlaan 200D, 3001 Leuven, Belgium*

† Electronic supplementary information (ESI) available: Synthetic procedures and analytical, UV/visible spectra in a variety of solvents, variable angle spectroscopic ellipsometry (VASE) data for films of chromophores and chromophore–polymer blends, HRS data analysis, computational methodology and additional DFT-calculated properties, poling data (plots of r_{33} *vs.* poling field), glass transition temperatures (T_g) as determined by differential scanning calorimetry (DSC), decomposition temperatures (T_d) as determined by thermogravimetric analysis (TGA), and cyclic voltammetry methods and data. See DOI: 10.1039/d1mh01206a

computing, sensor technology, and ultra-broadband signal processing at GHz–THz bandwidths.[1–6] Over the past decade, considerable progress has been made with respect to plasmonic-organic hybrid (POH)[2,3,5,7–9] and silicon-organic hybrid (SOH)[10–19] technologies affording higher bandwidth (>500 GHz),[20] smaller footprints (<20 μm^2), better energy efficiency (<100 attojoule/bit),[10,21] as well as dramatically lower $V_\pi L$ (the π-voltage–length product).[5,22] State-of-the-art POH and SOH platforms combine the high intrinsic EO activity of organic chromophores with the tight confinement and improved overlap of electrical and optical fields achievable in nanophotonic devices, enabling ultra-compact, low-voltage devices permitting chip-scale integration with CMOS electronics.[9,23–25] Achieving groundbreaking performance requires synergistic innovation from rational design of organic electro-optic (OEO) materials to device engineering and advancements in communication systems. As the active component for the Pockels effect, OEO materials offer coefficients up to 1000 pm V^{-1}, with commercial materials producing over 300 pm V^{-1} (>10× lithium niobate), femtosecond (<30 fs) response times, and wide compatibilities to a variety of integration platforms and device structures.[26–34] OEO materials can also be easily integrated into devices by low-cost, high-throughput methods such as spin-coating, micro-dispensing, or ink-jet printing. The EO activity of organic materials is derived from second-order nonlinear optical (NLO) properties of the chromophores and is proportional to the product of chromophore hyperpolarizability (β), electric field poling-induced acentric order of the chromophores ($\langle\cos^3\theta\rangle$), and chromophore number density (ρ_N).[34–36] In past a decade, EO performance has been improved *via* strategies such as site-isolation, self-assembly, chromophore blending, and charge blocking layers (CBLs) to enhance the $\rho_N\langle\cos^3\theta\rangle$ value of bulk materials.[26,28,31,33,37–49] Recent work[50,51] has also shown substantial increases in hyperpolarizability due to theory-guided design, after years of little increase in β of reported chromophores.

Modern density functional theory (DFT) methods provide excellent prediction for linear/nonlinear optical properties of NLO chromophores and better understanding of structure–property relationships.[25,52–54] Combining large-scale computation and theory-driven search, novel chromophore structures can be presented with enhanced hyperpolarizability while keeping dipole moment and band gap within acceptable constraints.[53,55] In this work, a new series of NLO chromophores were demonstrated by using a bis(arylamino) hybrid (BAH) electron donor (Fig. 1). Hyperpolarizabilities were predicted *via* DFT calculations[25,54,56] in chloroform with implicit solvent environments, and measured *via* hyper-Rayleigh scattering (HRS)[57–59] measurements in chloroform. These experiments demonstrate large improvements in β and slight redshifts in their main charge-transfer (CT) band (29 nm to 45 nm) compared to the widely used JRD1.[28,51] The chromophores have been engineered with bulky groups to prevent aggregation due to dipolar interactions. The presence of side-chain bulky groups was also helpful to improve chromophore solubility and film-forming property as well as reduce absorption.[28,39,60] To realize a highly acentric alignment ($\langle\cos^3\theta\rangle$), strong electric fields were applied to the OEO thin films. To suppress the leakage current and get a more uniform electric field, titanium dioxide (TiO_2) and hafnium dioxide (HfO_2) thin films have been utilized as CBLs.[28,61–63] The high dielectric constants of TiO_2 and HfO_2 allow the absolute majority of the poling and AC modulation field to be applied effectively across the micron-thick OEO layer. For electric field poling, the poled BAH13 films showed a significantly enhanced r_{33} value of 650 ± 110 pm V^{-1} on TiO_2, higher than neat JRD1,[28] which has a large r_{33} value (560 ± 90 pm V^{-1}).[28] The best r_{33} value (1100 ± 100 pm V^{-1}) of BAH13 was achieved by using HfO_2 as CBL, which is comparable to the performance of BAY1 but with greatly decreased absorption at communication wavelengths.[50]

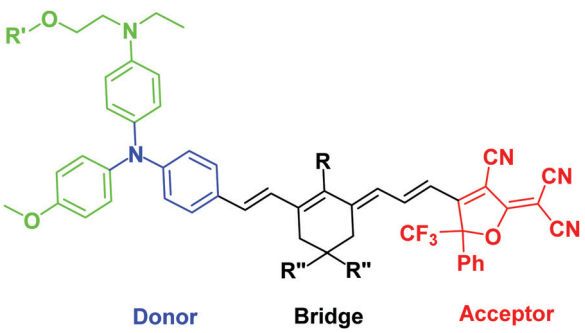

Fig. 1 Generic structure of a "BAH" chromophore, showing the donor (primary donor in blue, secondary donors in green), bridge, and acceptor.

2. Results and discussion

A key benefit of OEO materials *versus* most other NLO materials is that their structures have a broad parameter space for optimization of their optical and electronic properties. This has led to an evolution of structural design—guided by theory and computational modeling—to optimize EO performance. This evolution is illustrated in Table 1 with chromophore JRD1 as a starting point. JRD1 is based on the popular CLD-type chromophore structure using a dialkylamine donor, and ring-locked tetraene π-bridge, and a CF_3-Ph-tricyanofuran acceptor. Virtually all the best OEO device results have used CLD-type chromophores. The key modification introduced with JRD1 was two sterically bulky *tert*-butyldiphenylsilyl (TBDPS) groups, which permitted the chromophore to be processed neat (without polymer host) and still pole efficiently, reaching record high r_{33} in bulk and in-device. The performance of JRD1 was later translated to a crosslinkable material, HLD, which could provide similar performance with long-term thermal stability.[32] Despite the success of optimizing CLD-type chromophores, EO performance reached a limit that could only be improved by increasing β or through radically different design approaches such as sequential synthesis. After screening numerous design modifications, we discovered a class of molecules highlighted by BTP7 that had a powerful electron

Table 1 Progression of chromophore structures and how modifications effect key EO parameters

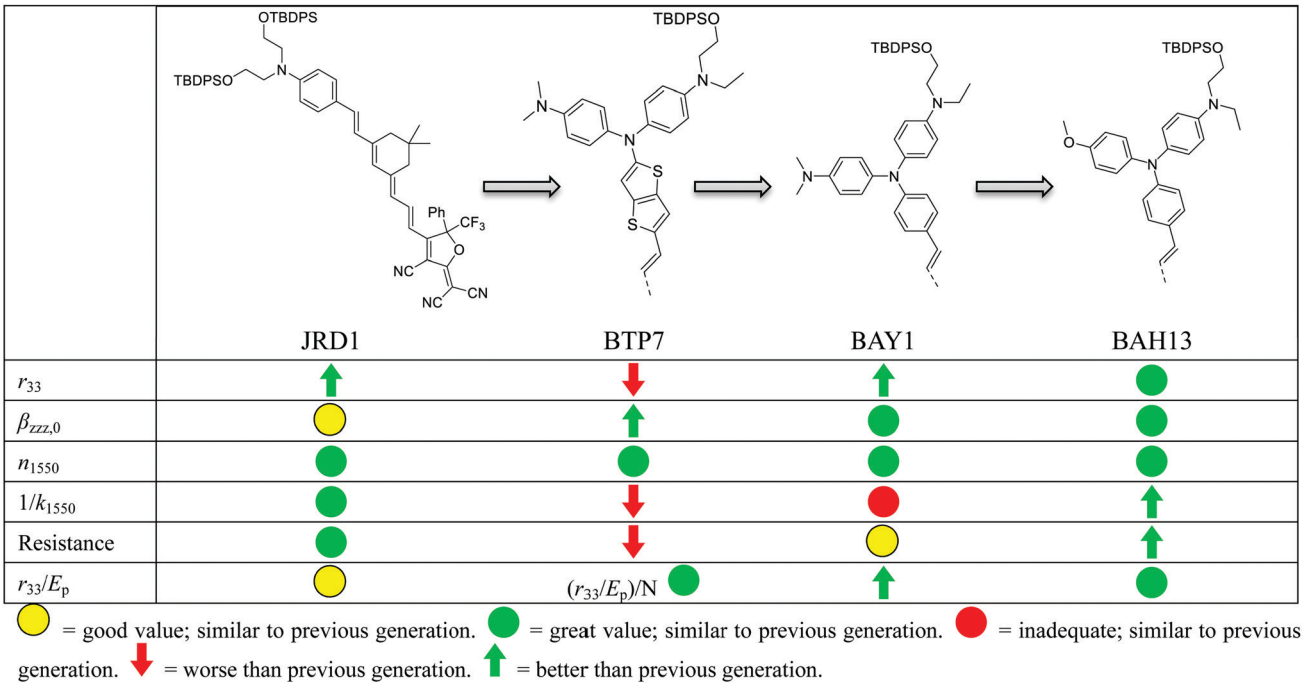

donor and huge enhancement in $\beta_{zzz,0}$ (β tensor component parallel to the dipole moment of the chromophore).[51] While this chromophore displayed excellent poling efficiency at low concentration, consistent with expectations for a higher $\beta_{zzz,0}$ material, the transmittance ($1/k$) in the near IR was too low and the resistance was too low to permit poling as a neat material, and therefore r_{33} was not ultimately improved. The next modification kept the strong donor but increased aromatic character in the donor-bridge transition to better balance the donor. The result was chromophore BAY1, which exhibited improved resistance that permitted poling as a neat material and record high $r_{33} > 1000$ pm V^{-1}, which is twice the EO coefficient of JRD1 and even higher than $BaTiO_3$.[64] However, the transmittance in the near IR was still lower than desired so another modification was needed. This paper introduces a new modification intended to increase the transmittance to an acceptable level for hybrid devices while maintaining ultra-high r_{33}, high $\beta_{zzz,0}$, high n, high resistance, and the good physical properties of the previous generation of chromophores. We synthesized three variants of the BAH structure shown in Fig. 2 that had different sterically bulky side-chain or bridge units. BAH13 is substituted with two pendant TBDPS groups, one on the donor end and one on the bridge. BAH-BB shares the same donor structures with BAH13 and includes rigid naphthyl and fluorenyl units on either side of the bridge designed to provide site isolation (reduce aggregation and anti-parallel dipolar coupling).[30] BAH-FD

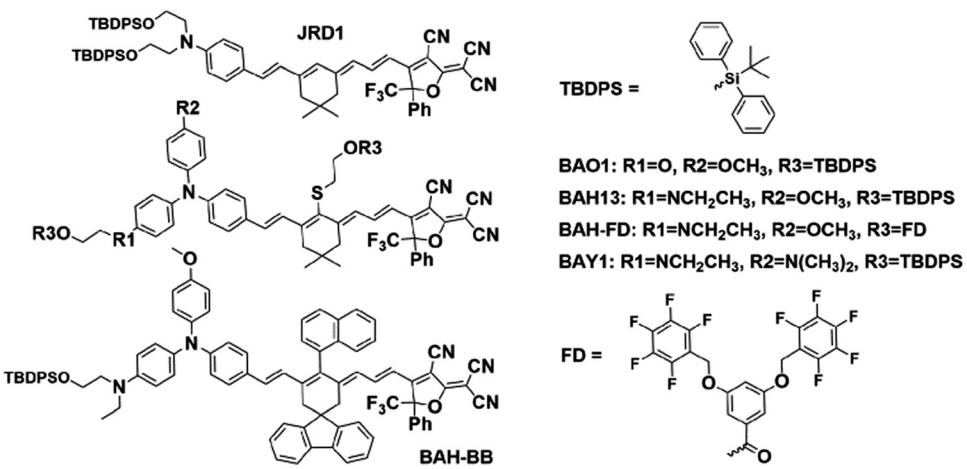

Fig. 2 Chromophore structures in this study.

was functionalized with fluoroaromatic dendrons (FD), which have been shown to blueshift the absorbance band and thereby reduce the absorption coefficient in the near IR. FD units are also known to promote favorable, cooperative intermolecular interactions in OEO materials resulting in increased poling performance.[26,33,42,65,66] We also synthesized a BAH variant for exploring relative substitution effects on the secondary electron-donating groups (BAO1). Full synthetic details, characterization and official IUPAC names[67] can be found in the ESI.†

The UV-vis-NIR spectra of chromophores were measured in six solvents with varying dielectric constants and as thin films (Table S1 and Fig. S11, ESI†). Three BAH chromophores share the same donor–π bridge–acceptor (D–π–A) structure, which results in the similar absorption maxima (λ_{max}) data and solvatochromic behavior. In chloroform, the (λ_{max}) of BAH chromophores showed large redshifts (by 41–57 nm) relative to JRD1 in the primary charge transfer band. λ_{max} is a good proxy for electron donor strength, and the redshift is evidence of the stronger electron-donating strength of (4-dialkylaminophenyl)(4-alkyloxyphenyl)phenyl-amino group (Table 3 and Fig. 3a). BAH chromophore absorbance in chloroform is blue shifted (by 61–77 nm) relative to BAY1 indicating that the BAH donor is intermediate between JRD1 and BAY1. BAO1 has the most blue shifted λ_{max} (772 nm) in chloroform in the set, even more so than JRD1, confirming that the weaker donating ability of 4-alkoxyphenyl. The trends in donor strength are confirmed by highest-occupied molecular orbital (HOMO) estimations from cyclic voltammetry (Fig. 3c and Fig. S18 and Table S3, ESI†). The side chains connected to the conjugated bridge of BAH-FD and BAH-BB have a slight effect on the π-system and therefore allow us to fine tune the linear- and nonlinear optical properties. BAH-BB has a slight blueshift (8 nm) in chloroform relative to BAH13. BAH-FD has a 16 nm blueshift in chloroform relative to BAH13, which is partially ascribed to the quadrupolar interactions between perfluorinated aromatic rings and electron-rich segments of the chromophore π-system. Neat thin films had the same trends in λ_{max} as in chloroform solution. These data serve as a guide for how to reduce optical loss in devices relative to BAY1.

The refractive index (n) and extinction coefficients (k) of unpoled films of neat chromophores and binary chromophore blends were measured using variable angle spectroscopic ellipsometry (VASE) (Table 2 and Fig. S12, ESI†). n_{1310} ranges from 1.96–1.81, and n_{1550} ranges from 1.87–1.75 for the BAH chromophores, BAO1, and their blends. BAH13 and BAH-BB have n values (n_{1310} = 1.95, 1.96, respectively) at the high end of the range. This observation is consistent with the general trend of refractive index increasing with number density and resonance effects. n values for BAH13 are very comparable to JRD1 and just a few percent lower than BAY1. The higher index of neat chromophore is significant in that the Pockels effect figure-of-merit (FOM) n^3r_{33} has a cubic dependence on n, such that small index increases can lead to significant increases in performance. The measured refractive index values were used to calculate r_{33} in EO poling tests. The BAH chromophores

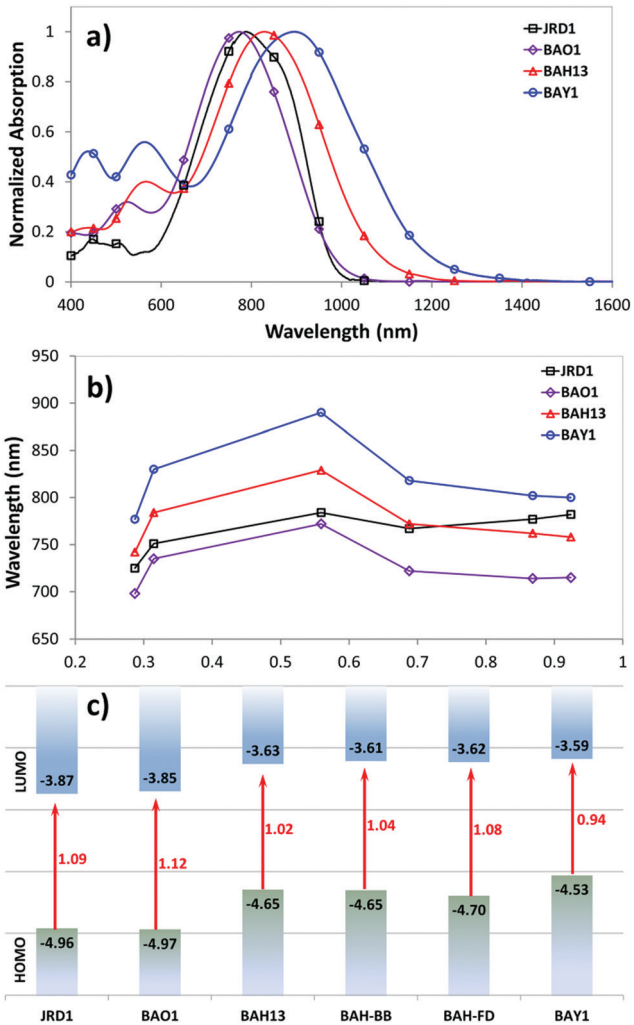

Fig. 3 (a) Normalized UV-vis-NIR spectra of chromophores in chloroform. (b) λ_{max} *vs.* solvent polarity on the Reichardt scale ($(\varepsilon - 1)/(\varepsilon + 2)$) spanning a range of dielectric constants from 1,4-dioxane (ε = 2.2) to acetonitrile (ε = 37.5). (c) HOMO from cyclic voltammetry (CV) and LUMO energy levels and thin film optical energy gaps, in eV; LUMO = HOMO (CV) + band gap (optical).

Table 2 Optical constants

Sample	n_{1310}	n_{1550}	k_{1310}	k_{1550}
100 wt% JRD1	1.91	1.84	0.00010	0.000018
100% BAY1	2.02	1.90	0.133	0.0255
100 wt% BAO1	1.84	1.79	0.00099	0.000042
100 wt% BAH13	1.94	1.85	0.02126	0.001
100 wt% BAH-BB	1.96	1.87	0.02906	0.00271
100 wt% BAH-FD	1.81	1.75	0.00695	0.00041
1 : 1 BAH-BB : BAH13	1.95	1.86	0.03395	0.00381
3 : 1 BAH-FD : BAH13	1.84	1.78	0.00891	0.000504

exhibited low k values that were ~10 to 50 times lower than BAY1, approximately equal to that of DLD164, the prior highest-performing chromophore in POH devices,[55] and within the loss threshold for POH devices (k_{1550} ~ 0.0055 = 0.19 dB μm^{-1}).[55] With the presence of FD groups, BAH-FD has greatly reduced

k values at telecommunication wavelengths compared with the other BAH chromophores.

Femtosecond HRS[59] measurements were performed in chloroform solution using a custom-built setup at KU Leuven. Measurements were performed using a fundamental wavelength of 1300 nm and a repetition rate of 80 MHz. HRS intensity was corrected for absorption using a Beer–Lambert correction at the second harmonic wavelength. Resonance effects were approximated using the damped two-level model (TLM) and a linewidth (γ) of 0.1 eV (for details see ESI†). HRS results of BAH13, BAO1, and previously published comparison molecules are summarized in Table 3 (BAH-BB and BAH-FD were excluded since these two chromophores have the same D–π–A system and substitution points as BAH13 and likely have similar hyperpolarizabilities). DFT calculations were also employed to evaluate the theoretical values and compare with experiment. The hyperpolarizabilities of JRD1, BAY1, and BTP7 have been measured with the same methods and reported in our previous work.[50,51] BAH13 exhibited a very large $\beta_{zzz,0}$ that was a more than 2.5-fold improvement over JRD1 and only ~10% less than BAY1. This BAH13 β is consistent with observations of λ_{max} and the HOMO levels being intermediate between JRD1 and BAY1, but more similar to BAY1. BAO1 has an enhanced $\beta_{zzz,0}$, 1.7 times that of JRD1, which is larger than expectations based on the computed $\beta_{zzz,0}$, and the experimental λ_{max} and HOMO level.

Thin film devices of neat and binary chromophores sandwiched between indium tin oxide (ITO) and glass were prepared to evaluate their bulk EO activity. OEO films were spin cast from 8–10 wt% chromophores into 1,1,2-trichloroethane (TCE). To achieve higher and more uniform electric fields, thin films of TiO_2 or HfO_2 were used as CBLs between ITO and the OEO material. CBL layers were deposited by either sol–gel,[61,62,68,69] electron beam physical vapor deposition (PVD), or atomic layer deposition (ALD) methods. Thin film devices were poled under DC electric fields (E_p) ranging from 20 to 90 V μm^{-1} with a heating rate of 10 °C per minute under nitrogen. During poling, the current and voltage across the device were collected along with an *in situ* r_{33} analysis at 1310 nm by the Teng–Man ellipsometric method.[70,71] After cooling down below 35 °C, the poling field was removed, then r_{33} values were measured. The average poling efficiencies (r_{33}/E_p) were determined by linear fitting of the electro-optic activity (in pm V^{-1}) *versus* E_p. Higher poling efficiency represents better performance of translating microscopic hyperpolarizability into macroscopic EO response. The poling results are shown in Fig. 4, Fig. S10 (ESI†) and summarized in Table 4.

BAO1 and BAH13 displayed excellent film-forming properties on ITO and on all CBLs. A remarkable poling efficiency (6.9 ± 0.3 nm^2 V^{-2}) was achieved in the neat BAH13 devices, which is an approximately 2-fold improvement over neat JRD1 performance. The best performing neat BAH13 device without a CBL also afforded a very large r_{33} value of 410 ± 30 pm V^{-1}, which is higher than some of the best OEO materials in the literatures. However, due to large leakage currents at high poling fields, the average poling fields on neat BAH13 devices with no barrier layer were limited to <60 V μm^{-1}. CBLs were used to minimize leakage current and maximize achievable poling fields. TiO_2 has been demonstrated as an effective CBL due to its large band gap, large dielectric constant, and excellent thin film processibility; we used layers of 20 nm (PVD or ALD) or 100 nm (sol–gel) in our devices. The neat BAO1 and BAH13 devices on TiO_2 exhibited slight increases in poling efficiency relative to the devices without CBL. It is notable that the neat BAH13 on TiO_2 achieved a poling efficiency increase of 0.8 nm^2 V^{-2} and a very large r_{33} value of 650 ± 110 pm V^{-1}, which is higher than the state-of-art JRD1 performance (560 ± 90 pm V^{-1}). While the increase in slope was of marginal statistical significance (p = 0.116 for a two-tailed T-test, 0.058 for one-tailed), the TiO_2 CBL enabled us of higher poling voltages and higher maximum EO activity. HfO_2 has also been adopted as a CBL due to its large dielectric constant, larger band gap than TiO_2, and high resistivity. Greatly reduced leakage currents were observed for the poling of neat BAH13 on HfO_2, improving the actual poling fields to higher than 80 V μm^{-1}. The neat BAH13 on HfO_2 showed the highest performance, with poling efficiencies of 11.6 ± 0.7 nm^2 V^{-2} and a record-high r_{33} value of 1100 ± 100 pm V^{-1}, which is comparable with the best value of neat BAY1 and approximate to 2-fold enhancement compared to the previous highest reported OEO material JRD1.

BAH-BB and BAH-FD exhibited poorer film-forming characteristics as neat materials, with cracking upon drying leading to device failure from short or open circuit conditions

Table 3 Linear and nonlinear optical properties of chromophores

Sample	λ_{max} (nm)	TLM[a] factor	μ[b] (D)	$\beta_{zzz,1300}$[c]	$\beta_{zzz,0}$[c]	$\beta_{zzz,0}/\beta_{JRD1}$	Comp.[d] $\beta_0/\beta_{0,JRD1}$
JRD1	784	3.13	31	3330 ± 50	1060 ± 20	1 ± 0.02	1
BAY1	890	2.11	30.2	6420 ± 90	3040 ± 40	2.87 ± 0.04	1.47
BAO1	772	3.76	26	6769 ± 630	1800 ± 170	1.70 ± 0.16	0.95
BAH13	829	2.69	28.6	7207 ± 298	2680 ± 110	2.53 ± 0.10	1.16
BAH-BB	821	2.66	26.2	—	—	—	1.17
BAH-FD	813	2.77	—	—	—	—	—

[a] The damped two-level model factor used to correct for resonance effects on β (for details, see ESI). [b] Dipole moment, M062X/6-31+G(d) calculation in polarizable continuum model (PCM) implicit solvent. [c] HRS – femtosecond HRS at 1300 nm ($\beta_{zzz,1300}$) in $CHCl_3$, extrapolation to zero frequency ($\beta_{zzz,0}$) using damped TLM (0.1 eV linewidth). Hyperpolarizabilities in 10^{-30} esu. Reference against solvent ($CHCl_3$, using Campo *et al.* (2009) value of $\beta_{zzz,0} \sim 0.44 \times 10^{-30}$ esu).[59] [d] Computational predictions – M062X/6-31+G(d) in PCM $CHCl_3$ at zero frequency, analytic differentiation, 2-carbon truncation on inactive side chains.

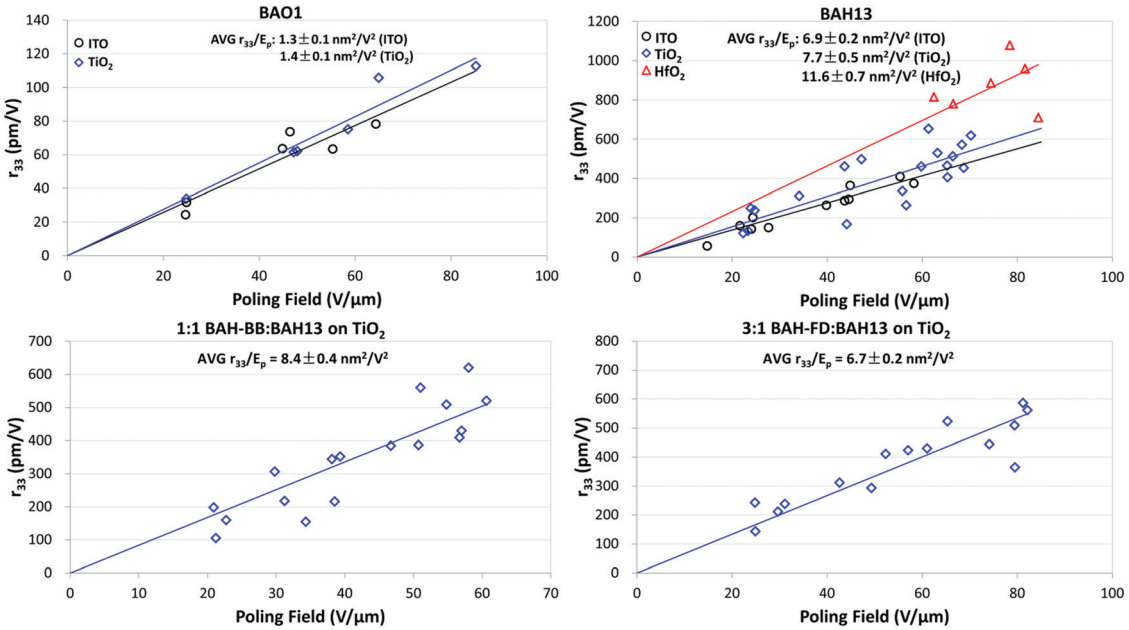

Fig. 4 Poling curves for BAH chromophores (plots of r_{33} *vs.* poling field). E_p is the average of poling fields at poling temperature and cooling down to 35 °C.

Table 4 Electric field poling data for EO chromophores in bulk devices

Sample	ρ_N[a]	CBL	Poling temp. (°C)	r_{33}/E_p[b] (nm^2 V^{-2})	Max. r_{33} (pm V^{-1})	Max. n^3r_{33} (pm V^{-1})
100% BAO1	4.43	None	82–85	1.3 ± 0.1	78 ± 8	490 ± 50
		TiO_2	82–85	1.4 ± 0.1	113 ± 8	700 ± 50
100% BAH13	4.35	None	81–85	6.9 ± 0.2	410 ± 30	3000 ± 200
		TiO_2	81–85	7.7 ± 0.5	650 ± 100	4700 ± 800
		HfO_2	75–79	11.6 ± 0.7	1100 ± 100	7800 ± 1000
3 : 1 BAH-FD : BAH13	3.46	TiO_2	65–68	6.7 ± 0.3	590 ± 50	3700 ± 300
1 : 1 BAH-BB : BAH13	4.46	TiO_2	100–103	8.4 ± 0.3	620 ± 60	4600 ± 400
100% JRD1	5.33	BCB	~93	3.4 ± 0.2	560 ± 70	3900 ± 500
100% BAY1	4.30	TiO_2	86–91	16.6 ± 0.5	1100 ± 100	9000 ± 1100

[a] Number density (×10^{20} molecules per cm^3, assumes mass density of 1 g cm^{-3}). [b] Average from multiple poling experiments (Fig. 4 and Fig. S10, ESI).

during poling. Film forming could be greatly improved by blending with BAH13; 25 wt% and 50 wt% BAH13 were blended with BAH-FD and BAH-BB, respectively. Due to the impressive poling results of neat BAH13 on TiO_2, the following evaluations of 1 : 1 BAH-BB : BAH13 and 3 : 1 BAH-FD : BAH13 blends were performed on TiO_2, as well. The poling efficiency of 3 : 1 BAH-FD : BAH13 was 6.7 ± 0.3 nm^2 V^{-2}, nearly a 2-fold improvement over neat JRD1 performance. This relatively lower poling efficiency is attributed to the low chromophore number density (3.46 × 10^{20} molecules per cm^3) of 3 : 1 BAH-FD : BAH13 compared with other BAH materials (4.35–4.46 × 10^{20} molecules per cm^3). Also due to the lower chromophore number density, 3 : 1 BAH-FD : BAH13 device achieved higher maximum poling field (~80 V μm^{-1}) leading to a large r_{33} value of 590 ± 50 pm V^{-1}, and a low absorbance at telecommunication wavelengths. Due to the very high T_g (127 °C) of BAH-BB, 1 : 1 BAH-BB : BAH13 was poled at 100–103 °C, and showed a higher poling efficiency of 8.4 ± 0.3 nm^2 V^{-2} and yielded a maximum r_{33} of 620 ± 60 pm V^{-1}.

BAH13 was also evaluated in-device on a POH platform. POH devices feature large bandwidths, small footprint, low power consumption, and can be fabricated on top of CMOS electronics as a post-process.[9] In POH phase modulators, light is coupled from a silicon strip waveguide into a metal–insulator–metal slot waveguide and converted to a surface plasmon polariton (SPP) mode at the gold surface. The SPPs propagate along the gold-dielectric interface. Plasmonics allows light confinement below the diffraction limit as well as enhanced light–matter interaction. The slot waveguide is filled with the OEO material, and the device is poled in a manner similar to bulk devices: the modulator is heated to the T_g, then an electric field is applied to the gold waveguide walls that serve as poling electrodes. The Pockels effect of the poled OEO material is used to encode an electrical signal on the phase of the propagating SPPs. At the end of the plasmonic waveguide, the phase modulated SPPs are converted back to photonic modes of the output silicon waveguide by the second taper structure. In this work, the phase plasmonic phase modulators are integrated in an imbalanced

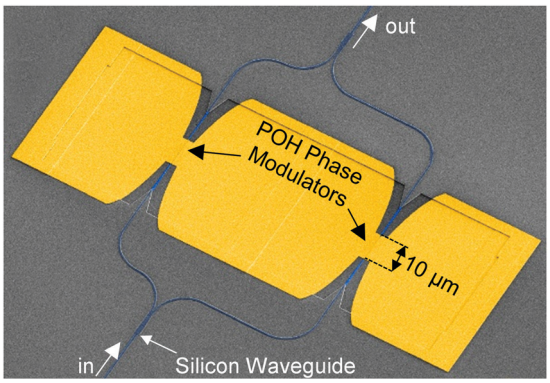

Fig. 5 Colorized scanning-electron microscope picture of a POH Mach–Zehnder modulator.

silicon–photonic push–pull Mach–Zehnder geometry,[55] Fig. 5, in which two phase modulators are oppositely driven. At an applied voltage V_π, each phase modulator produces opposite quarter-wave phase shifts leading to complete destructive interference between the two arms, switching the modulator from the on- to the off-state. The EO performance at 1550 nm is determined in 10 μm long modulators with 80 and 105 nm wide slots operating in the 15–70 GHz range. To measure the on–off voltage V_π, the wavelength-dependent intensity transfer function was recorded while applying DC voltages between ±1 V in steps of 0.5 V. By measuring the voltage-dependent spectral shift of transmission spectrum,[55] V_π was measured to be 4.8 V and 6.5 V for 80 and 105 nm wide slots, respectively. Based on these drive voltages, the devices had voltage–length products $V_\pi L$ of 48 V μm and 65 V μm (Table 5). The electro-optic coefficient for BAH13 calculates to a maximum r_{33} of 197 and 208 pm V^{-1} in the modulators with 80 and 105 nm slot width, respectively. Further discussion on the differences between r_{33} values obtained in bulk devices at 1310 nm and narrow slot POH devices operating at 1550 nm is included in the ESI.† Based on these calculations and assuming negligible differences between 105 and 100 nm slots, this suggests a 1.7× improvement in r_{33} and a 1.8× improvement in n^3r_{33} over JRD1 in POH devices.[55] The best $V_\pi L$ product of BAH13 is 48 V μm, which is comparable to the best values previously reported.[55] However, the present value was achieved in a much wider waveguide (80 nm *vs.* 40 nm), making fabrication more accessible. As the improvement was consistent with predictions using finite difference eigenmode (FDE) calculations (ESI†) on POH slot waveguides using our recent methodology,[72] it suggests that $V_\pi L < 20$ V μm could be obtained in narrower slots (Fig. 6), though potentially requiring CBLs and further optimization of poling protocols.

Table 5 POH Mach–Zehnder modulator device results at 1550 nm

	BAH13		JRD1	
w_{slot} (nm)	80	105	100	150
r_{33} (pm V^{-1})	197	208	123	156
n^3r_{33} (pm V^{-1})	1251	1321	730	925
$V_\pi L$ (V μm)	48	65	112	146

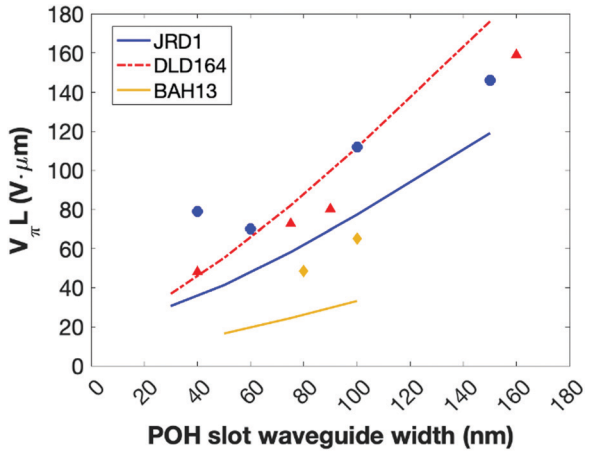

Fig. 6 Comparison of measured (symbols) and computationally predicted (lines) $V_\pi L$ values for JRD1, DLD164,[39,55] and BAH13 at 1550 nm in a POH MZI configuration. Measured values for JRD1 and DLD164 are from ref. 55; predictions use the methodology in ref. 72. No CBLs were included in the waveguide calculations. Calculations are discussed in ESI.†

3. Conclusions

We synthesized and characterized four chromophores derived from theory-guided design and optimized to achieve high EO activity with acceptable loss and processibility; the highest-performing chromophore was also evaluated in POH devices. Due to the fine-tuned electron donating ability, the derived chromophores exhibited large molecular hyperpolarizabilities and controllable redshifts of absorption. To prevent dipolar interaction-induced aggregation, the chromophores were functionalized with side-chain bulky groups on donor and bridge moieties. In bulk devices BAH chromophores showed significantly improved EO performance including r_{33} values and poling efficiencies. Neat BAH13 devices with HfO_2 CBL produced a very large maximum r_{33} value of 1100 ± 100 pm V^{-1} at 1310 nm. This r_{33} is equivalent to BAY1, with a much-improved absorption coefficient making it practical for use in EO modulators. 3 : 1 BAH-FD : BAH13 blends showed a lower poling efficiency of 6.7 ± 0.3 nm^2 V^{-2} and a greatly reduced absorbance, which is important to the performance of modulators. 1 : 1 BAH-BB : BAH13 has the highest poling efficiency of 8.4 ± 0.4 nm^2 V^{-2} and an improved T_g > 100 °C. The neat BAH13 was evaluated in POH modulators, achieving $V_\pi L < 50$ V μm in substantially wider slots than prior record devices. In POH modulators, BAH13 exhibited high r_{33} values of 208 pm V^{-1} at 1550 nm, substantially exceeding the performance of prior chromophores evaluated in equivalent device architectures.

Author contributions

LEJ, DLE, and BHR conceived the project. LEJ performed electronic structure calculations, electrodynamics calculations, and associated data analysis. LEJ, DLE, HX, and BHR contributed to design of novel compounds. HX synthesized and performed

structural, linear optical, electro-optic, and thermal characterization on all compounds. DLE performed VASE characterization and assisted with other techniques and DLE and SRH contributed characterization protocols and assisted with interpretation of data. YdC and WVG performed all hyper-Rayleigh Scattering spectroscopy experiments and associated data analysis; KC and LEJ assisted with HRS data interpretation. SRH performed PVD and ALD depositions for CBLs. WH designed the POH devices and managed testing and in-device characterization; EDL and NM fabricated the POH devices, and MD performed poling experiments in POH devices. HX, LEJ, and DLE wrote the initial manuscript and led revision in response to reviewer comments. LEJ and DLE managed the project. BHR, LRD, KC and JL provided research-group level supervision, mentoring, and funding. All authors edited and approved the manuscript.

Conflicts of interest

Competing Financial Interest Disclosure. Some work in this study is related to technology described in patent applications filed by the University of Washington, ''Organic Electro-Optic Chromophores,'' International Application No. PCT/US2020/054081, which have been licensed by Nonlinear Materials Corporation (NLM). L. E. J. is a co-founder and part-time employee of NLM and an equity holder in NLM. S. R. H and D. L. E. are part-time employees of NLM and equity holders in NLM. B. H. R. is an advisor to NLM and an equity holder in NLM. The terms of this arrangement have been reviewed and approved by the University of Washington in accordance with its policies governing outside work and financial conflicts of interest in research. W. H. is a co-founder, full-time employee, and equity holder in Polariton Technologies AG, which is commercializing POH technology. E. D. L., N. M., and M. D. are full-time employees of Polariton Technologies AG. J. L. is an advisor to and equity holder in Polariton Technologies AG. All other authors declare no competing financial interests.

Acknowledgements

We gratefully acknowledge the financial support of the Air Force Office of Scientific Research (FA9550-19-1-0069), the National Science Foundation (IIP-2036514), the University of Washington College of Arts and Sciences, Flemish Fund for Scientific Research (FWO-V, G0A1817N), the University of Leuven (C16/16/003), EU-Project NEBULA (871658), and EU Project PlasmoniAC (871391). Part of this work was conducted at the Molecular Analysis Facility, a National Nanotechnology Coordinated Infrastructure (NNCI) site at the University of Washington, which is supported in part by funds from the National Science Foundation (awards NNCI-2025489, NNCI-1542101), the Molecular Engineering & Sciences Institute, and the Clean Energy Institute.

Notes and references

1 R. Bonjour, M. Burla, F. C. Abrecht, S. Welschen, C. Hoessbacher, W. Heni, S. A. Gebrewold, B. Baeuerle, A. Josten, Y. Salamin, C. Haffner, P. V. Johnston, D. L. Elder, P. Leuchtmann, D. Hillerkuss, Y. Fedoryshyn, L. R. Dalton, C. Hafner and J. Leuthold, *Opt. Express*, 2016, **24**, 25608–25618.

2 M. Ayata, Y. Fedoryshyn, W. Heni, B. Baeuerle, A. Josten, M. Zahner, U. Koch, Y. Salamin, C. Hoessbacher, C. Haffner, D. L. Elder, L. R. Dalton and J. Leuthold, *Science*, 2017, **358**, 630–632.

3 C. Haffner, D. Chelladurai, Y. Fedoryshyn, A. Josten, B. Baeuerle, W. Heni, T. Watanabe, T. Cui, B. Cheng, S. Saha, D. L. Elder, L. R. Dalton, A. Boltasseva, V. M. Shalaev, N. Kinsey and J. Leuthold, *Nature*, 2018, **556**, 483–486.

4 Y. Salamin, I.-C. Benea-Chelmus, Y. Fedoryshyn, W. Heni, D. L. Elder, L. R. Dalton, J. Faist and J. Leuthold, *Nat. Commun.*, 2019, **10**, 5550.

5 S. Ummethala, T. Harter, K. Koehnle, Z. Li, S. Muehlbrandt, Y. Kutuvantavida, J. Kemal, P. Marin-Palomo, J. Schaefer, A. Tessmann, S. K. Garlapati, A. Bacher, L. Hahn, M. Walther, T. Zwick, S. Randel, W. Freude and C. Koos, *Nat. Photonics*, 2019, **13**, 519–524.

6 I.-C. Benea-Chelmus, Y. Salamin, F. F. Settembrini, Y. Fedoryshyn, W. Heni, D. L. Elder, L. R. Dalton, J. Leuthold and J. Faist, *Optica*, 2020, **7**, 498.

7 C. Hoessbacher, A. Josten, B. Baeuerle, Y. Fedoryshyn, H. Hettrich, Y. Salamin, W. Heni, C. Haffner, C. Kaiser, R. Schmid, D. L. Elder, D. Hillerkuss, M. Moller, L. R. Dalton and J. Leuthold, *Opt. Express*, 2017, **25**, 1762–1768.

8 W. Heni, B. Baeuerle, H. Mardoyan, F. Jorge, J. M. Estaran, A. Konczykowska, M. Riet, B. Duval, V. Nodjiadjim, M. Goix, J.-Y. Dupuy, M. Destraz, C. Hoessbacher, Y. Fedoryshyn, H. Xu, D. L. Elder, L. R. Dalton, J. Renaudier and J. Leuthold, *J. Lightwave Technol.*, 2020, **38**, 2734–2739.

9 U. Koch, C. Uhl, H. Hettrich, Y. Fedoryshyn, C. Hoessbacher, W. Heni, B. Baeuerle, B. I. Bitachon, A. Josten, M. Ayata, H. Xu, D. L. Elder, L. R. Dalton, E. Mentovich, P. Bakopoulos, S. Lischke, A. Krüger, L. Zimmermann, D. Tsiokos, N. Pleros, M. Möller and J. Leuthold, *Nat. Electron.*, 2020, **3**, 338–345.

10 S. Koeber, R. Palmer, M. Lauermann, W. Heni, D. L. Elder, D. Korn, M. Woessner, L. Alloatti, S. Koenig, P. C. Schindler, H. Yu, W. Bogaerts, L. R. Dalton, W. Freude, J. Leuthold and C. Koos, *Light-Sci. Appl.*, 2015, **4**, e255–e255.

11 C. Koos, J. Leuthold, W. Freude, M. Kohl, L. Dalton, W. Bogaerts, A. L. Giesecke, M. Lauermann, A. Melikyan, S. Koeber, S. Wolf, C. Weimann, S. Muehlbrandt, K. Koehnle, J. Pfeifle, W. Hartmann, Y. Kutuvantavida, S. Ummethala, R. Palmer, D. Korn, L. Alloatti, P. C. Schindler, D. L. Elder, T. Wahlbrink and J. Bolten, *J. Lightwave Technol.*, 2016, **34**, 256–268.

12 C. Kieninger, Y. Kutuvantavida, D. L. Elder, S. Wolf, H. Zwickel, M. Blaicher, J. N. Kemal, M. Lauermann,

S. Randel, W. Freude, L. R. Dalton and C. Koos, *Optica*, 2018, **5**, 739.
13 C. Kieninger, C. Fullner, H. Zwickel, Y. Kutuvantavida, J. N. Kemal, C. Eschenbaum, D. L. Elder, L. R. Dalton, W. Freude, S. Randel and C. Koos, *Opt. Express*, 2020, **28**, 24693–24707.
14 L. Alloatti, R. Palmer, S. Diebold, K. P. Pahl, B. Q. Chen, R. Dinu, M. Fournier, J. M. Fedeli, T. Zwick, W. Freude, C. Koos and J. Leuthold, *Light-Sci. Appl.*, 2014, **3**, e173–e173.
15 R. Palmer, S. Koeber, D. L. Elder, M. Woessner, W. Heni, D. Korn, M. Lauermann, W. Bogaerts, L. Dalton, W. Freude, J. Leuthold and C. Koos, *J. Lightwave Technol.*, 2014, **32**, 2726–2734.
16 M. Lauermann, S. Wolf, P. C. Schindler, R. Palmer, S. Koeber, D. Korn, L. Alloatti, T. Wahlbrink, J. Bolten, M. Waldow, M. Koenigsmann, M. Kohler, D. Malsam, D. L. Elder, P. V. Johnston, N. Phillips-Sylvain, P. A. Sullivan, L. R. Dalton, J. Leuthold, W. Freude and C. Koos, *J. Lightwave Technol.*, 2015, **33**, 1210–1216.
17 C. Kieninger, Y. Kutuvantavida, H. Miura, J. N. Kemal, H. Zwickel, F. Qiu, M. Lauermann, W. Freude, S. Randel, S. Yokoyama and C. Koos, *Opt. Express*, 2018, **26**, 27955–27964.
18 S. Wolf, H. Zwickel, W. Hartmann, M. Lauermann, Y. Kutuvantavida, C. Kieninger, L. Altenhain, R. Schmid, J. Luo, A. K. Jen, S. Randel, W. Freude and C. Koos, *Sci. Rep.*, 2018, **8**, 2598.
19 S. Ummethala, J. N. Kemal, A. S. Alam, M. Lauermann, A. Kuzmin, Y. Kutuvantavida, S. H. Nandam, L. Hahn, D. L. Elder, L. R. Dalton, T. Zwick, S. Randel, W. Freude and C. Koos, *Optica*, 2021, **8**, 511.
20 M. Burla, C. Hoessbacher, W. Heni, C. Haffner, Y. Fedoryshyn, D. Werner, T. Watanabe, H. Massler, D. L. Elder, L. R. Dalton and J. Leuthold, *APL Photonics*, 2019, **4**, 056106.
21 W. Heni, Y. Fedoryshyn, B. Baeuerle, A. Josten, C. B. Hoessbacher, A. Messner, C. Haffner, T. Watanabe, Y. Salamin, U. Koch, D. L. Elder, L. R. Dalton and J. Leuthold, *Nat. Commun.*, 2019, **10**, 1694.
22 C. Haffner, W. Heni, Y. Fedoryshyn, J. Niegemann, A. Melikyan, D. L. Elder, B. Baeuerle, Y. Salamin, A. Josten, U. Koch, C. Hoessbacher, F. Ducry, L. Juchli, A. Emboras, D. Hillerkuss, M. Kohl, L. R. Dalton, C. Hafner and J. Leuthold, *Nat. Photonics*, 2015, **9**, 525–528.
23 L. R. Dalton, B. H. Robinson, D. L. Elder, A. F. Tillack and L. E. Johnson, Presented in part at the SPIE Organic Photonics + Electronics, 2017, DOI: 10.1117/12.2278795.
24 W. Heni, Y. Kutuvantavida, C. Haffner, H. Zwickel, C. Kieninger, S. Wolf, M. Lauermann, Y. Fedoryshyn, A. F. Tillack, L. E. Johnson, D. L. Elder, B. H. Robinson, W. Freude, C. Koos, J. Leuthold and L. R. Dalton, *ACS Photonics*, 2017, **4**, 1576–1590.
25 B. Robinson, L. Johnson, D. Elder, A. Kocherzhenko, C. Isborn, C. Haffner, W. Heni, C. Hoessbacher, Y. Fedoryshyn, Y. Salamin, B. Baeuerle, A. Josten, M. Ayata, U. Koch, J. Leuthold and L. R. Dalton, *J. Lightwave Technol.*, 2018, **36**, 5036–5047.
26 T. D. Kim, J. W. Kang, J. Luo, S. H. Jang, J. W. Ka, N. Tucker, J. B. Benedict, L. R. Dalton, T. Gray, R. M. Overney, D. H. Park, W. N. Herman and A. K. Jen, *J. Am. Chem. Soc.*, 2007, **129**, 488–489.
27 T.-D. Kim, J. Luo, Y.-J. Cheng, Z. Shi, S. Hau, S.-H. Jang, X.-H. Zhou, Y. Tian, B. Polishak, S. Huang, H. Ma, L. R. Dalton and A. K. Y. Jen, *J. Phys. Chem. C*, 2008, **112**, 8091–8098.
28 W. W. Jin, P. V. Johnston, D. L. Elder, A. F. Tillack, B. C. Olbricht, J. S. Song, P. J. Reid, R. M. Xu, B. H. Robinson and L. R. Dalton, *Appl. Phys. Lett.*, 2014, **104**, 243304.
29 W. W. Jin, P. V. Johnston, D. L. Elder, K. T. Manner, K. E. Garrett, W. Kaminsky, R. M. Xu, B. H. Robinson and L. R. Dalton, *J. Mater. Chem. C*, 2016, **4**, 3119–3124.
30 D. L. Elder, C. Haffner, W. Heni, Y. Fedoryshyn, K. E. Garrett, L. E. Johnson, R. A. Campbell, J. D. Avila, B. H. Robinson, J. Leuthold and L. R. Dalton, *Chem. Mater.*, 2017, **29**, 6457–6471.
31 H. Xu, J. Liu, J. Liu, C. Yu, Z. Zhai, G. Qin and F. Liu, *Mater. Chem. Front.*, 2020, **4**, 168–175.
32 H. J. Xu, F. G. Liu, D. L. Elder, L. E. Johnson, Y. de Coene, K. Clays, B. H. Robinson and L. R. Dalton, *Chem. Mater.*, 2020, **32**, 1408–1421.
33 X. H. Zhou, J. D. Luo, S. Huang, T. D. Kim, Z. W. Shi, Y. J. Cheng, S. H. Jang, D. B. Knorr, R. M. Overney and A. K.-Y. Jen, *Adv. Mater.*, 2009, **21**, 1976–1981.
34 L. R. Dalton, P. A. Sullivan and D. H. Bale, *Chem. Rev.*, 2010, **110**, 25–55.
35 P. A. Sullivan and L. R. Dalton, *Acc. Chem. Res.*, 2009, **43**, 10–18.
36 J. Y. Wu, Z. A. Li, J. D. Luo and A. K. Y. Jen, *J. Mater. Chem. C*, 2020, **8**, 15009–15026.
37 P. A. Sullivan, H. Rommel, Y. Liao, B. C. Olbricht, A. J. Akelaitis, K. A. Firestone, J. W. Kang, J. Luo, J. A. Davies, D. H. Choi, B. E. Eichinger, P. J. Reid, A. Chen, A. K. Jen, B. H. Robinson and L. R. Dalton, *J. Am. Chem. Soc.*, 2007, **129**, 7523–7530.
38 S. J. Benight, D. B. Knorr Jr., L. E. Johnson, P. A. Sullivan, D. Lao, J. Sun, L. S. Kocherlakota, A. Elangovan, B. H. Robinson, R. M. Overney and L. R. Dalton, *Adv. Mater.*, 2012, **24**, 3263–3268.
39 D. L. Elder, S. J. Benight, J. S. Song, B. H. Robinson and L. R. Dalton, *Chem. Mater.*, 2014, **26**, 872–874.
40 M. Li, S. Huang, X.-H. Zhou, Y. Zang, J. Wu, Z. Cui, J. Luo and A. K. Y. Jen, *J. Mater. Chem. C*, 2015, **3**, 6737–6744.
41 J. Wu, J. Luo, N. Cernetic, K. Chen, K.-S. Chiang and A. K. Y. Jen, *J. Mater. Chem. C*, 2016, **4**, 10286–10292.
42 Z. A. Li, P. Chen, Y. Xie, Z. Li and J. Qin, *Adv. Electron. Mater.*, 2017, **3**, 1700138.
43 J. Wu, B. Wu, W. Wang, K. S. Chiang, A. K.-Y. Jen and J. Luo, *Mater. Chem. Front.*, 2018, **2**, 901–909.
44 F. Liu, S. Chen, S. Mo, G. Qin, C. Yu, W. Zhang, W.-J. Shi, P. Chen, H. Xu and M. Fu, *J. Mater. Chem. C*, 2019, **7**, 8019–8028.
45 F. Liu, M. Zhang, H. Xiao, Y. Yang, H. Wang, J. Liu, S. Bo, Z. Zhen, X. Liu and L. Qiu, *J. Mater. Chem. C*, 2015, **3**, 9283–9291.

46 H. Zhang, H. Xiao, F. Liu, F. Huo, Y. He, Z. Chen, X. Liu, S. Bo, L. Qiu and Z. Zhen, *J. Mater. Chem. C*, 2017, **5**, 1675–1684.
47 H. Zhang, Y. Yang, H. Xiao, F. Liu, F. Huo, L. Chen, Z. Chen, S. Bo, L. Qiu and Z. Zhen, *J. Mater. Chem. C*, 2017, **5**, 6704–6712.
48 Y. He, L. Chen, H. Zhang, Z. Chen, F. Huo, B. Li, Z. Zhen, X. Liu and S. Bo, *J. Mater. Chem. C*, 2018, **6**, 1031–1037.
49 Z. Chen, A. Zhang, H. Xiao, F. Huo, Z. Zhen, X. Liu and S. Bo, *Dyes Pigm.*, 2020, **173**, 107876.
50 H. Xu, D. L. Elder, L. E. Johnson, Y. de Coene, S. R. Hammond, W. Vander Ghinst, K. Clays, L. R. Dalton and B. H. Robinson, *Adv. Mater.*, 2021, 2104174.
51 H. Xu, L. E. Johnson, Y. de Coene, D. L. Elder, S. R. Hammond, K. Clays, L. R. Dalton and B. H. Robinson, *J. Mater. Chem. C*, 2021, **9**, 2721–2728.
52 L. E. Johnson, L. R. Dalton and B. H. Robinson, *Acc. Chem. Res.*, 2014, **47**, 3258–3265.
53 L. Johnson, D. Elder, A. Kocherzhenko, A. Tillack, C. Isborn, L. Dalton and B. Robinson, Presented in part at the SPIE Organic Photonics + Electronics, 2018.
54 L. Johnson, H. Xu, Y. de Coene, D. Elder, K. Clays, L. Dalton and B. Robinson, Presented in part at the SPIE Nanoscience + Engineering, 2019.
55 W. Heni, C. Haffner, D. L. Elder, A. F. Tillack, Y. Fedoryshyn, R. Cottier, Y. Salamin, C. Hoessbacher, U. Koch, B. Cheng, B. Robinson, L. R. Dalton and J. Leuthold, *Opt. Express*, 2017, **25**, 2627–2653.
56 L. Johnson, H. Xu, S. Hammond, D. Elder, S. Benight, Y. de Coene, J. Hesse-Withbroe, K. Clays, L. Dalton and B. Robinson, Presented in part at the SPIE Nanoscience + Engineering, 2020.
57 K. Clays and A. Persoons, *Phys. Rev. Lett.*, 1991, **66**, 2980–2983.
58 K. Clays and A. Persoons, *Rev. Sci. Instrum.*, 1992, **63**, 3285–3289.
59 J. Campo, F. Desmet, W. Wenseleers and E. Goovaerts, *Opt. Express*, 2009, **17**, 4587–4604.
60 A. F. Tillack and B. H. Robinson, *J. Opt. Soc. Am. B*, 2016, **33**, E121–E129.
61 M. J. Alam and D. C. Cameron, *J. Sol–Gel Sci. Technol.*, 2002, **25**, 137–145.
62 S. Huang, T. D. Kim, J. D. Luo, S. K. Hau, Z. W. Shi, X. H. Zhou, H. L. Yip and A. K. Y. Jen, *Appl. Phys. Lett.*, 2010, **96**, 243311.
63 Y. Enami, B. Yuan, M. Tanaka, J. Luo and A.-Y. Jen, *Appl. Phys. Lett.*, 2012, **101**, 123509.
64 S. Abel, F. Eltes, J. E. Ortmann, A. Messner, P. Castera, T. Wagner, D. Urbonas, A. Rosa, A. M. Gutierrez, D. Tulli, P. Ma, B. Baeuerle, A. Josten, W. Heni, D. Caimi, L. Czornomaz, A. A. Demkov, J. Leuthold, P. Sanchis and J. Fompeyrine, *Nat. Mater.*, 2019, **18**, 42–47.
65 H. Xu, D. L. Elder, L. E. Johnson, B. H. Robinson and L. R. Dalton, *ACS Appl. Mater. Interfaces*, 2019, **11**, 21058–21068.
66 X. Zang, G. Liu, Q. Li, Z. A. Li and Z. Li, *Macromolecules*, 2020, **53**, 4012–4021.
67 ChemAxon, *Marvin 21.9*, 2021, https://chemaxon.com/.
68 T. Nishide, S. Honda, M. Matsuura and M. Ide, *Thin Solid Films*, 2000, **371**, 61–65.
69 H. Shimizu, T. Sato, S. Konagai, M. Ikeda, T. Takahashi and T. Nishide, *Jpn. J. Appl. Phys.*, 2007, **46**, 4209–4214.
70 C. C. Teng and H. T. Man, *Appl. Phys. Lett.*, 1990, **56**, 1734–1736.
71 Y. Shuto and M. Amano, *J. Appl. Phys.*, 1995, **77**, 4632–4638.
72 L. E. Johnson, D. L. Elder, S. J. Benight, A. F. Tillack, S. R. Hammond, L. R. Dalton and B. H. Robinson, Presented in part at the SPIE Organic Optics + Photonics, 2021.

